



# Provenance and Climatic Implications of the Middle-Pleistocene Loess Deposit, Southern China

Qingbin Fan<sup>1,2</sup>, Jie Liao<sup>1\*</sup>, Yan Li<sup>3</sup>, Wei Ye<sup>4</sup>, Tao Wang<sup>1</sup> and Xiao Feng<sup>1,2</sup>

<sup>1</sup>Key Laboratory of Desert and Desertification, Northwest Institute of Eco-Environment and Resources, Chinese Academy of Sciences, Lanzhou, China, <sup>2</sup>University of Chinese Academy of Sciences, Beijing, China, <sup>3</sup>College of Forestry, Nanjing Forestry University, Nanjing, China, <sup>4</sup>College of Geography and Environmental Sciences, Zhejiang Normal University, Jinhua, China

## OPEN ACCESS

### Edited by:

Xiangjun Liu,  
Northwest Normal University, China

### Reviewed by:

Ruijie Lu,  
Beijing Normal University, China  
Zhiyong Ling,  
Chinese Academy of Sciences, China

### \*Correspondence:

Jie Liao  
liaojie@lzb.ac.cn

### Specialty section:

This article was submitted to  
Quaternary Science, Geomorphology  
and Paleoenvironment,  
a section of the journal  
Frontiers in Earth Science

**Received:** 19 March 2021

**Accepted:** 07 May 2021

**Published:** 31 May 2021

### Citation:

Fan Q, Liao J, Li Y, Ye W, Wang T and  
Feng X (2021) Provenance  
and Climatic Implications of the  
Middle-Pleistocene Loess Deposit,  
Southern China.  
*Front. Earth Sci.* 9:682875.  
doi: 10.3389/feart.2021.682875

The middle-Pleistocene Xiashu loess deposit in the lower reaches of the Yangtze River (LRYR), southern China, may yield evidence with significant climatic and environmental significance. However, its provenance remains controversial. In this study, grain size analysis, and quartz grain surface microtextural and morphological observations, enabled comparison of the provenance of loess in the LRYR with those on the Loess Plateau in northern China. The results show that the grain size characteristics of the Xiashu loess do not follow the coarse-fine NW-SE trend in northern China, and the surface microtextures of the quartz grains in the Xiashu loess are distinctly different from those on the Loess Plateau in northern China, indicating that the loess deposits in the two regions have different provenances. The Gobi Desert in inland northwestern China are not considered as the primary provenance of the Xiashu loess. Instead, the adjacent floodplains in the LRYR, the alluvial plains of the Huai River and the Yellow River to the north during glacial periods are suggested as the dominant source materials for the Xiashu loess. Under the background of middle-Pleistocene climate transition (MPT), regional aridity and a strengthened east Asian winter monsoon (driven by global cooling and the rapid uplift of the Tibetan Plateau) were considered as the primary drivers for the development of the Xiashu loess. The sustained eolian loess accumulation represent a regional response of the northern subtropical area of southern China to the MPT global cooling event at around 0.9 Ma.

**Keywords:** Xiashu loess, eolian, provenance, east Asian winter monsoon, global cooling

## INTRODUCTION

Global climate changes and their regional responses are receiving considerable research attention, with Quaternary climate evolution providing an important focus (Liu, 1985; Pye, 1987; Li et al., 2001a; Li et al., 2018a; Purtil et al., 2019; Westerhold et al., 2020). China is a typical monsoon-influenced country, the summer monsoon brings abundant water vapor to the continent, and the winter monsoon entrains and transports large volumes of dust, carrying it to the middle, east and south of China (Ding et al., 2019; Li et al., 2021a; Li et al., 2021b). The eolian dust deposited on the continent thus provides a basis for the reconstruction of environment in China. Such as the thick eolian loess deposit on the Chinese Loess Plateau (CLP) in northern China, which is regarded as a valuable sedimentary archive for Quaternary climate and environment changes. Systematic studies have revealed its sedimentation chronology, provenance, the process causing aridification in

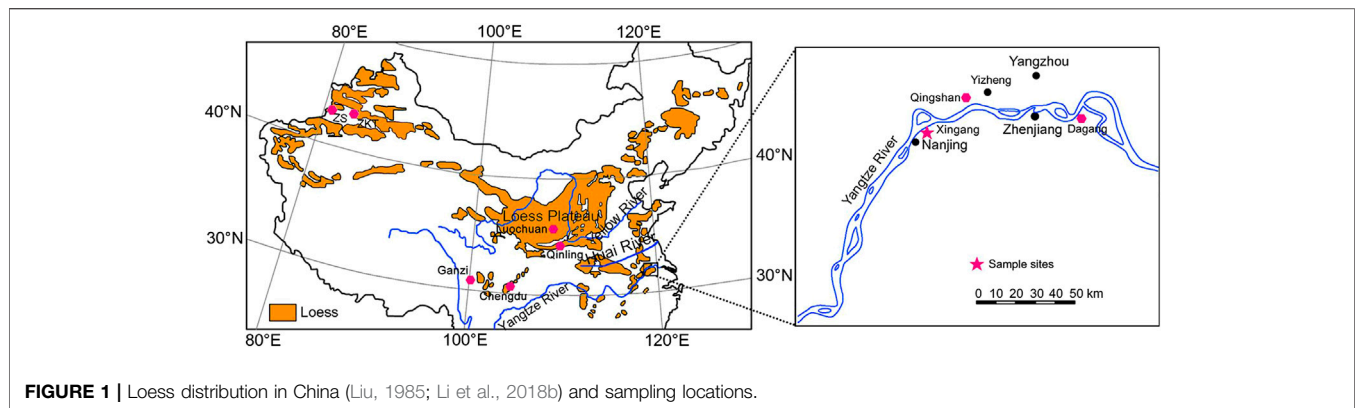


**FIGURE 1** | Loess distribution in China (Liu, 1985; Li et al., 2018b) and sampling locations.

northern China and the evolution of the east Asian monsoon climate (Liu, 1985; An et al., 1990; Guo, 2010; Ding et al., 2019). However, Quaternary loess deposits in China are not only distributed on the CLP, but also distributed in the northwest and northeast China, as well as the areas of Nanjing, Zhenjiang and Yangzhou in the lower reaches of the Yangtze River (LRYR) (Figure 1). In 1932, Siguang Li and Sen Zhu named the loess in the LRYR as Xiashu Loess according to the loess strata in Xiashu Town, Jiangsu Province (Hao et al., 2010). The Xiashu loess is located at the boundary of northern and southern China, in the north subtropics and at the southeast edge of the loess distribution area in China, a region that is sensitive to climate changes. The occurrence of dust deposition usually indicates an important climatic or environmental change in the source and/or deposition regions (Pye, 1995). Therefore, The development of the eolian Xiashu loess deposit in the LRYR of southern China may yield evidence with significant environmental implications.

Previous studies have focused on grain-size characteristics (Li et al., 1997; Li et al., 2001b; Qiao et al., 2003), environmental magnetism (Zhang et al., 2007; Zhang et al., 2009), clay mineral assemblage (Shi et al., 2005), sedimentary chronology (Qiao et al., 2003; Zhang et al., 2009; Hao et al., 2010; Li et al., 2018b) and chemical weathering (Yang et al., 2004; Chen et al., 2008) in order to study the sedimentary chronology, provenance and environmental significance of the Xiashu loess. In terms of its chronology, due to the limitations in the employed dating methods, dated materials and stratigraphic profiles, this issue has been debated for decades. Firstly some researchers suggested that the Xiashu loess was deposited in the late Pleistocene (Li et al., 1978; Wu, 1985; Zheng, 1999), whereas others suggested that the loess deposit began in the mid Pleistocene (Liu, 1985; Lai et al., 2001; Wu et al., 2006; Zhang et al., 2009). In recent years, new advances in magnetostratigraphy and optically stimulated luminescence (OSL) dating have constrained the age of the lower boundary of the Xiashu loess to approximately 0.9 Ma, representing the oldest age reported to date and is widely accepted (Qiao et al., 2003; Hao et al., 2010; Li et al., 2018b).

With regard to its origin, there are mainly two viewpoints: although eolian origin is becoming increasingly accepted, the material source area of the Xiashu loess remains controversial. A “distant-source” theory believes that the Xiashu loess originated from the Gobi Desert in inland northwestern China, analogous to

the loess deposit on the CLP; on the contrary, the “near-source” theory suggests that the loess materials were derived from the adjacent floodplains to the north of the Yangtze River and the Huai River system during glacial periods (Hao et al., 2010; Yang et al., 2017; Li et al., 2018b; Jiang et al., 2020; Wu et al., 2020). Different views on the origin of the Xiashu loess lead to contrasting environmental interpretations. The former interpretation implies that the development of the Xiashu loess was a consequence of increasing aridification in the northwest inland of China, coupled with the intensified east Asian winter monsoon linked to global cooling, uplift of the Tibetan Plateau and the consequent enhancement of the Siberian high pressure (Liu, 1985). The latter view considers the occurrence of the Xiashu loess to be an indicator of aridification in nearby north subtropical regions during glacial periods (Hao et al., 2010; Li et al., 2018b; Jiang et al., 2020). Therefore, identification the provenance of the Xiashu loess could provide new insights into the environmental implications of this valuable sedimentary archive and the driving factors of climate changes in the north subtropics area of southern China.

Aiming at the most controversial problem in study of the Xiashu loess, this paper reports field investigations of the Xingang (XG) profile, a typical Xiashu loess profile in Nanjing on south bank of the Yangtze River. After systematic sampling, the grain-size characteristics and quartz grain surface microtextures were analyzed, interpreted and compared with those on the CLP in northern China in order to find valid evidence for identifying its provenance. Our results may provide further data to support paleoenvironmental reconstruction for the LRYR in southern China.

## MATERIALS AND METHODS

### The Study Area and Sampling

The Xiashu loess deposit is widespread in the lower reaches of the Yangtze River (LRYR). This area is now situated in a warm-humid north subtropics monsoon climatic zone, with a mean annual precipitation of 1,000–1,200 mm, and a mean annual temperature of 15–17°C (Yang et al., 2017). In most cases, the Xiashu loess covers on the terraces along the Yangtze River and its tributaries.

**TABLE 1** | Stratigraphic description of the Xiashu loess profile in XG, Nanjing.

Layer	Depth(m)	color of the loess	description	description
1	0–3.6	Paleosol	Reddish-brown	Granular structure, loose, contains many plant roots
2	3.6–4.0	Loess	Pale brown	Contains black iron-manganese films, and is more strongly weathered than other loess layers
3	4.0–5.8	Paleosol	Reddish-brown	Granular structure, the upper texture is sticky and the lower texture is loose
4	5.8–9.0	Loess	Pale yellow	The texture is uniform, loose and porous, with vertical joints. Brown films are visible in the lower part
5	9.0–11	Loess	Brownish yellow	The texture is uniform, porous, and denser than the upper layer, with many iron manganese nodules in the lower part
6	11–13	Paleosol	Reddish-brown	Prismatic structure with dense texture, contains many black films
7	13–13.45	Paleosol	Reddish-brown	Prismatic structure with compact texture and plant roots
8	13.45–14.20	Loess	Brownish yellow	Large prismatic block structure, porous, with few films
9	14.20–15.30	Paleosol	Summer tan	Granular and compact in texture, with many films in the lower part, and large iron-manganese nodules
10	15.3-bottom not observed	Semi-weathered sandstone	Summer tan	Weathered bedrock materials, with iron-manganese nodules, gradually transiting downward to the bedrock

The Xiashu loess deposit accounts for 35–50% in the LRYR (Figure 1), especially prevalent on the hills, highlands, terraces, and other geomorphic units along the Yangtze River and its tributaries. In addition, loess also occurs on the Yangtze River Delta, the continental shelf and islands of the East China Sea. The elevation of the Xiashu loess exposures varies significantly, from over 60 m above sea level to 20 m below sea level. The thickness of the Xiashu loess reaches a maximum of over 50 m in Qingshan, Dagang and Zhenjiang. In Nanjing, the Xiashu loess deposit is distributed as platforms on the river terraces of the Yangtze River, with surface elevations of 30–40 m and thicknesses of approximately 20 m. The outcropping landforms of the Xiashu loess are mostly characterized by highlands and river terraces, and the underlying strata are mainly composed of gravel layers or Cretaceous sandstones. The loess strata are generally horizontal, slightly inclined, inconsistent with the bedrock inclination.

The Xingang (XG) profile (32° 08' 45.5"N, 118° 50' 51.6"E) (Figure 1) is located in the Xingang Development Zone on south bank of the Yangtze River, approximately 20 km northeast of Nanjing City, Jiangsu Province. The XG profile is a typical Xiashu loess profile exposed by engineering excavation. The profile is about 15.7 m in thickness, with interbedded loess and paleosol (Table 1), and has three steps dividing the profile into three distinct sections: from bottom to top, these are XG-1, XG-2 and XG-3, respectively. The complete profile has four paleosol layers and three loess layers (Table 1). A weathering crust and Cretaceous sandstone are visible in the lower part. A total of 81 samples were collected from bottom to top at equal intervals of 20 cm for grain-size analysis and quartz grain surface microtextural and morphological observations.

## Methods

### Grain Size

Grain size characteristics are mainly controlled by transportation mode and sedimentary environment. Therefore, grain size analysis is

often used to identify provenance and the sedimentary environment (Vandenberghe, 2013; Vandenberghe et al., 2018; Yang et al., 2019; Van Buuren et al., 2020). For the convenience of comparison with previous studies, the classification scheme used in this study is: sand (> 50 μm), silt (50–5 μm), coarse silt (50–10 μm), fine silt (10–5 μm), clay (< 5 μm) (Lei, 1998; Li et al., 2001b). The commonly used grain size parameter indexes include average grain size (Mz), standard deviation (Sd), skewness (Sk) and kurtosis (Kg). The mathematical calculation formula of particle size parameters are as follows (Folk and Ward, 1957; Yang et al., 2014):

$$Mz = \frac{\sum_{i=1}^n x_i f_i}{100}$$

$$Sd = \sqrt{\frac{\sum_{i=1}^n (x_i - Mz)^2 f_i}{100}}$$

$$Sk = \sqrt[3]{\frac{\sum_{i=1}^n (x_i - Mz)^3 f_i}{100 Sd^3}}$$

$$Kg = \sqrt[4]{\frac{\sum_{i=1}^n (x_i - Mz)^4 f_i}{100 Sd^4}}$$

The grain size analysis experiment was carried out in the geographic process laboratory, Zhejiang Normal University, using a Mastersizer 2000 laser grain size analyzer (Malvern, United Kingdom) with a measurement range of 0.01–2000 μm and an error of <2%. Samples for grain size analysis were pre-treated as follows. Samples were first boiled with 10% H<sub>2</sub>O<sub>2</sub> and 10% HCl to remove the organic matter and carbonate, respectively. Next, 0.5 mol/L (NaPO<sub>3</sub>)<sub>6</sub> was added as a dispersant, then the pretreated samples were ultrasonicated for 15 min before being analyzed.

### Fisher Linear Discriminant Analysis

Fisher linear discriminant analysis (FLDA) is a common classification method for multivariate statistical analysis, and is

**TABLE 2** | Equality test of group means.

Parameters	Wilks' lambda	F	Significance probability
Mz	0.262	286.586	0
Sd	0.02	5,079.284	0
Sk	0.042	2,334.562	0
Kg	0.203	401.401	0

widely used to identify various sedimentary environment. In this paper, we use FLDA to identify sedimentary environment based on statistical analysis of fluvial deposit (FD) and eolian deposit (ED) grain size parameters. The function we create is as follows.  $y = -1.138 \cdot Mz + 1.58 \cdot Sd - 0.781 \cdot Sk + 0.805 \cdot Kg$ , the threshold level is  $-4.5744$  (if  $y > -4.5744$ , they belong to ED; if  $y < -4.5744$ , they belong to FD).

In this study, we select a typical eolian loess profiles Zeketai (ZKT) profile in Xinjiang province, which is considered as a provenance for the loess on the CLP (Liu, 1985; Yang et al., 2014), and also selected Luochuan (LC) loess profile located on the central CLP, as well as Nantong (NT) profile (floodplain deposit) in the LRYR, which is considered to have played an important role in the accumulation of the Xiashu loess. To test the linear discriminant function created above, 215 typical eolian loess samples from ZKT profile and 33 typical floodplain deposit samples from NT profile were inputted into statistical software (SPSS) as ED and FD training sets respectively. All the significance probability values of the variable group mean are less than 0.001 (Table 2). Therefore, the four variables included in this discriminant analysis are all effective.

The Box's M test assesses the assumption of homogeneity of covariance matrices. This test is very sensitive to meet the assumption of multivariate normality. The statistical value of Box's M is 738.71 (Table 3), far greater than 0.05. Therefore, each of the covariance matrices can be considered equal. The significance probability of the F-test is 0.000, less than 0.05, indicating that the error judgment rate is minimal.

In order to verify the reliability of this model, sediment grain size parameters (Mz, Sd, Sk, and Kg) of eolian loess samples from ZKT profile, floodplain deposit samples from NT profile, and 57 eolian loess samples from LC profile were computed using the function. As shown in Table 3, all the eolian loess samples from ZKT profile and LC profile were identified as ED, resulting in an accuracy of 100% (Table 4). All the floodplain deposit samples from NT profile were identified as FD. Hence, the discriminant model is reliable.

### End-Member Modeling Analysis

End-member analysis is one of the most effective methods to study the transportation dynamics and sedimentary environment

**TABLE 3** | Box's M test results of equality covariance matrixes.

Boxe's M	F	
	Approx	Sig
738.71	70.049	0

(Vandenberghe, 2013; Ding et al. 2021), the grain size of the Xiashu loess was primarily controlled by source materials as well as transport dynamics and post-depositional weathering and pedogenesis (Liu, 1985). In this study, either we selected three or four endmembers,  $R^2 > 99\%$ , when we selected three endmembers, the correlation between endmembers  $> 0.4$ , while when we selected four endmembers, the correlation  $< 0.2$ . Therefore, it is reasonable to select four endmembers in this study (Figure 2).

### Quartz Grain Microtextures

Quartz minerals have high hardness, stable chemical properties and strong weathering resistance, leading to a variety of microtextures that can be well preserved on the surface of quartz grains. These microtextures are considered to reflect sedimentary history of the quartz grains, and can indicate the parent rock, transportation process, and depositional environment. Many researchers have therefore stated that quartz grain surface microtextures can be used to identify different sedimentary environments (Liu 1985; Pye K 1995; Helland et al. 1997; Mahaney & Kalm, 2000; Mahaney 2002; Guo et al. 2002; Qiao et al. 2003; Costa et al. 2012, Costa et al. 2013; Mahaney et al. 2014; Smith et al. 2018; Chen et al. 2019). On one hand, dish-shaped depressions, crescentic marks, upturned plates, meandering ridges and pockmarked surfaces are regarded as typical features of eolian quartz grains (Wang and Deonarine, 1985; Mahaney, 2002; Krinsley and Doornkamp, 2011; Costa et al., 2012, Costa et al., 2013). For example, dish-shaped depressions often occur in high-energy eolian environments where grains collide with each other. Pockmarks are typical characteristics of markings for eolian quartz grains, crowded pits result from collision with other grains during wind transportation, forming pockmarked surfaces. Upturned plates, which commonly occurred on edges of the grains that had good roundness, resulted from abrasion between grains in eolian environments. Meandering ridges are associated with eolian environments too (Wang and Deonarine, 1985; Mahaney, 2002). On the other hand, conchoidal fractures, V-shaped cracks, polished surfaces, triangular cracks, parallel striations, and grooves (straight and curved) are considered to be typical features for quartz grains from subaqueous environments (Wang and Deonarine, 1985; Mahaney et al., 2001; Mahaney, 2002; Sweet and Soreghanm, 2010; Vos et al., 2014; Smith et al., 2018). V-shaped cracks are considered to be developed by "grain-to-grain collisions" in subaqueous environments, where grains are triangular in shape and are non-oriented. Parallel striations result from "grain-to-grain scratches" in fluvial environments (Wang and Deonarine, 1985; Mahaney, 2002; Vos et al., 2014). Mahaney (2002) concluded that V-shaped cracks are the most common feature associated with fluvial environment.

In this study, quartz grain microtextures were observed under an S-4800 high-resolution field emission scanning electron microscope (SEM) produced by Hitachi (Japan) at the Institute of Physical Chemistry, Zhejiang Normal University. The extraction method for quartz grain before SEM observation was as follows:

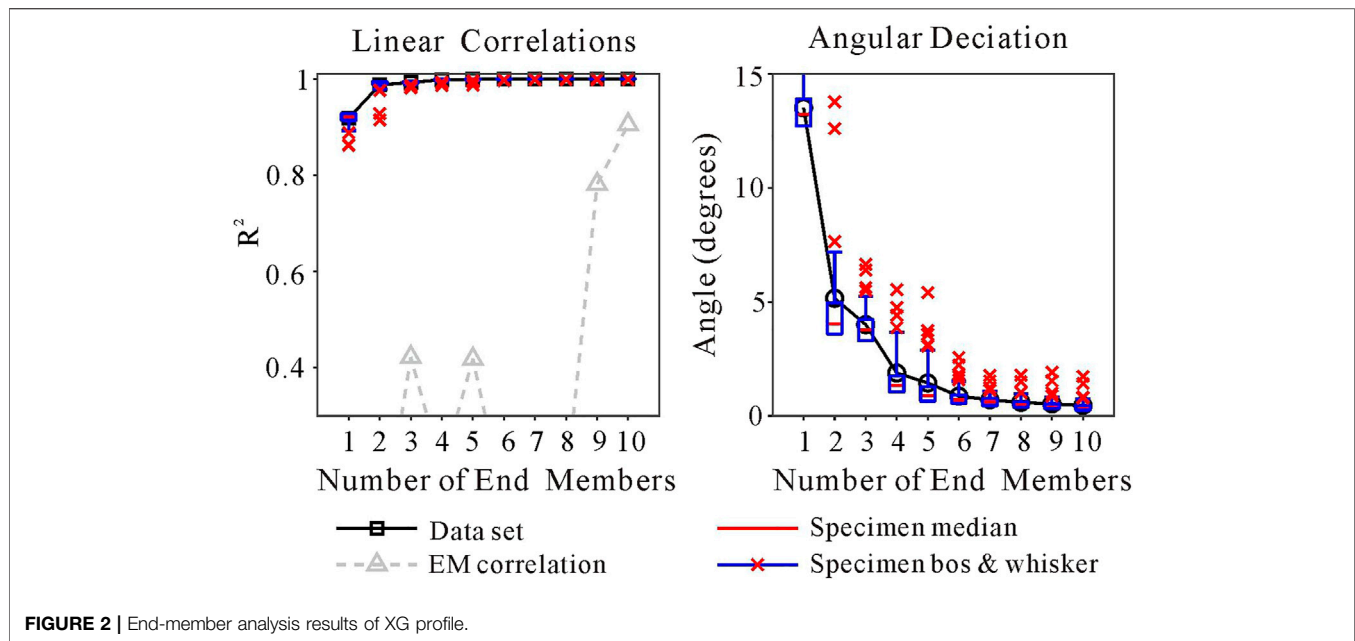


FIGURE 2 | End-member analysis results of XG profile.

- (1) To remove free iron, the dried sample was placed in centrifuge tube with sodium dithionite, sodium citrate (0.3 mol/L) and sodium bicarbonate solution (1 mol/L) and heated in a water bath. The solution was then separated by centrifuge until clear.
- (2) The quartz minerals were separated and purified by the potassium pyrosulfate melting-fluorosilicic acid immersion method. After removing the free iron, the samples were mixed with potassium pyrosulfate powder and heated in a muffle furnace for 1 h (initial temperature 350°C, then 650°C from 20 min to the end). The heated samples were transferred to a beaker, and HCL solution (1:3) was added to the heating plate to dissolve the frit. After separation by centrifuge, the samples were dried in the oven. The samples were then soaked in fluorosilicic acid for 3 days. The solution was centrifuged and the clear liquid was removed three days later. The residue was dried, and the quartz grains with highest purity were extracted.

According to Tsoar and Pye (1987), dust particles  $<20\ \mu\text{m}$  can be transported over wide altitudinal ranges and long distances by long-term suspension. Therefore, we observed grains that were large than  $20\ \mu\text{m}$  and finer than  $20\ \mu\text{m}$  under the Scanning Electron Microscope (SEM), and 20 quartz grains (including 10 grains  $>20\ \mu\text{m}$  and 10 grains  $<20\ \mu\text{m}$ ) in each sample were selected in XG profile, and a total of 1,620 quartz grains were observed and counted.

## RESULTS

### Grain Size Characteristics of XG Profile

The grain-size analysis results show that the Xiashu loess in XG, Nanjing mainly consists of fine components  $<50\ \mu\text{m}$ . No particles  $>250\ \mu\text{m}$  were found in any samples. The content of sand grains ( $>50\ \mu\text{m}$ ) is low (range 5.5–8%, average 6.84%) (Table 5). The silt

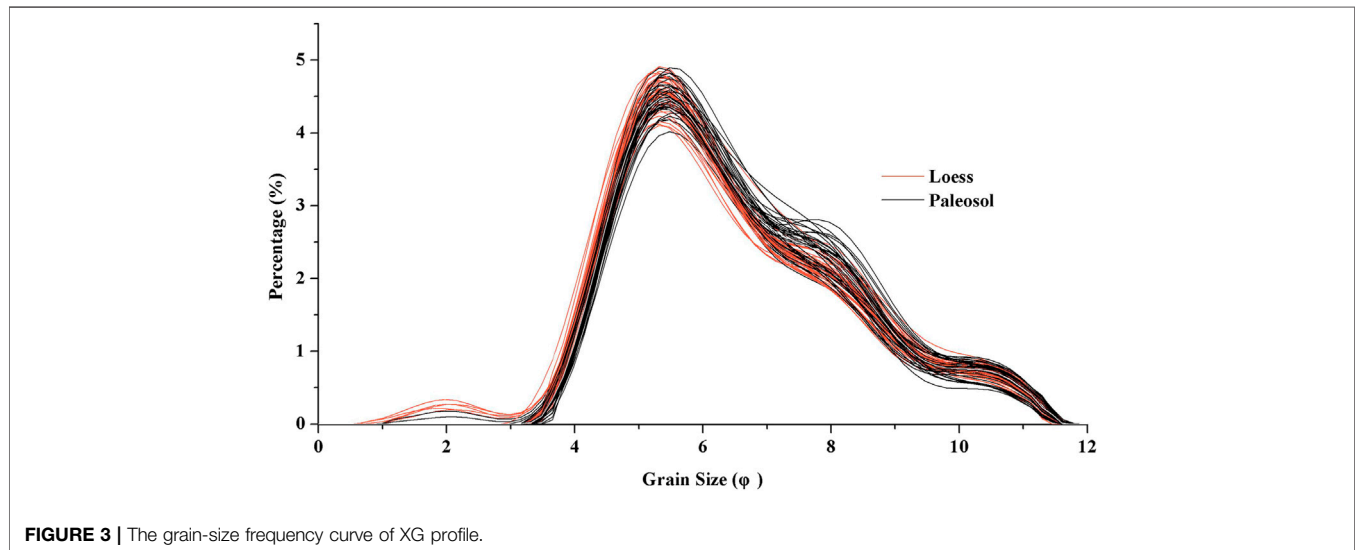
( $50\text{--}5\ \mu\text{m}$ ) content varies from 62.41 to 75.02% (mean 68.82%). The average content of coarse silt ( $50\text{--}10\ \mu\text{m}$ ) is 53.57%; this is the dominant grain size both in XG profile and for the loess on the CLP, and is regarded as a characteristic grain size in eolian loess deposit (Liu, 1985; Guo et al., 2002; Qiao et al., 2003). The average fine silt ( $10\text{--}5\ \mu\text{m}$ ) content is 15.25%. Finally, clay ( $<5\ \mu\text{m}$ ) is the sub-dominant grain size (average 24.34%), second only to the coarse silt in XG profile (Table 5).

The average grain size ( $M_z$ ) of samples from XG profile varied from  $6.23\phi$  to  $6.68\phi$  (mean  $6.47\phi$ ) (Table 5). The sorting coefficient ( $S_d$ ) ranges from 1.52 to 1.79, with a mean value of 1.65, indicating a poor sorting; skewness ( $S_k$ ) varies from 0.54 to 0.84 (mean 0.67), indicating positive skewness; kurtosis ( $K_g$ ) ranges from 2.53 to 3.13 (mean 2.80), showing that most samples are sharply peaked.

The grain-size frequency curve (Figure 3) of XG profile is characterized by a major peak and other three small peaks. The major peak is located near  $5.5\phi$ , with other three small peaks near  $2\phi$ ,  $8\phi$ , and  $10.5\phi$  respectively. The small peak near  $2\phi$  indicates that the XG profile contains a certain amount of coarse-grained materials, namely sand content. The two small peaks near  $8\phi$  and  $10.5\phi$  suggest that the Xiashu loess contains more fine-grained materials in the two places. On the whole, the frequency curve is characterized by a striking high content of sand, fine silt and clay component, which is unusual for pure windblown loess, the small peak near  $8\phi$  probably indicate a small amount of far - distant component, and the small peak near  $10.5\phi$  may indicate the existence of a large amount of clay component in XG profile. The frequency curve of XG profile suggests that the Xiashu loess is probably a admixture composed of near - source materials and long - transport materials. On one hand, it is likely that the Xiashu loess is primarily a near - source deposit, so the sand, silt and clay were mixed together during transportation, resulting in more sand materials in XG profile, and these materials have undergone a strong

**TABLE 4** | The verification of the discriminant function.

Profile codes	No. of samples	Actual category	Discriminant results		Accuracy (%)
			ED	FD	
ZKT	215	ED	215	0	100
NT	33	FD	0	33	100
LC	57	ED	57	0	100

**FIGURE 3** | The grain-size frequency curve of XG profile.**TABLE 5** | Grain size composition and Grain size parameters of XG profile.

Profile		Grain size composition/% grain size parameters										
		<5	5–10	10–50	>10	>20	>50	>250	Mz	Sd	Sk	kg
XG	Min	21.45	12.85	44.65	52.75	34.54	5.5	0.00	6.23	1.52	0.54	2.53
	Max	27.24	17.46	57.84	65.59	46.69	8.00	0.00	6.68	1.79	0.84	3.13
	Mean value	24.34	15.25	53.57	60.51	38.92	6.84	0.00	6.47	1.65	0.67	2.80

weathering and pedogenesis process in the warm-humid north subtropical monsoon climate after deposition, causing a obviously high content of clay component. On the other hand, the join up of a small amount of far - distant fine materials caused a small peak near  $8\phi$  and a poor sorting in XG profile.

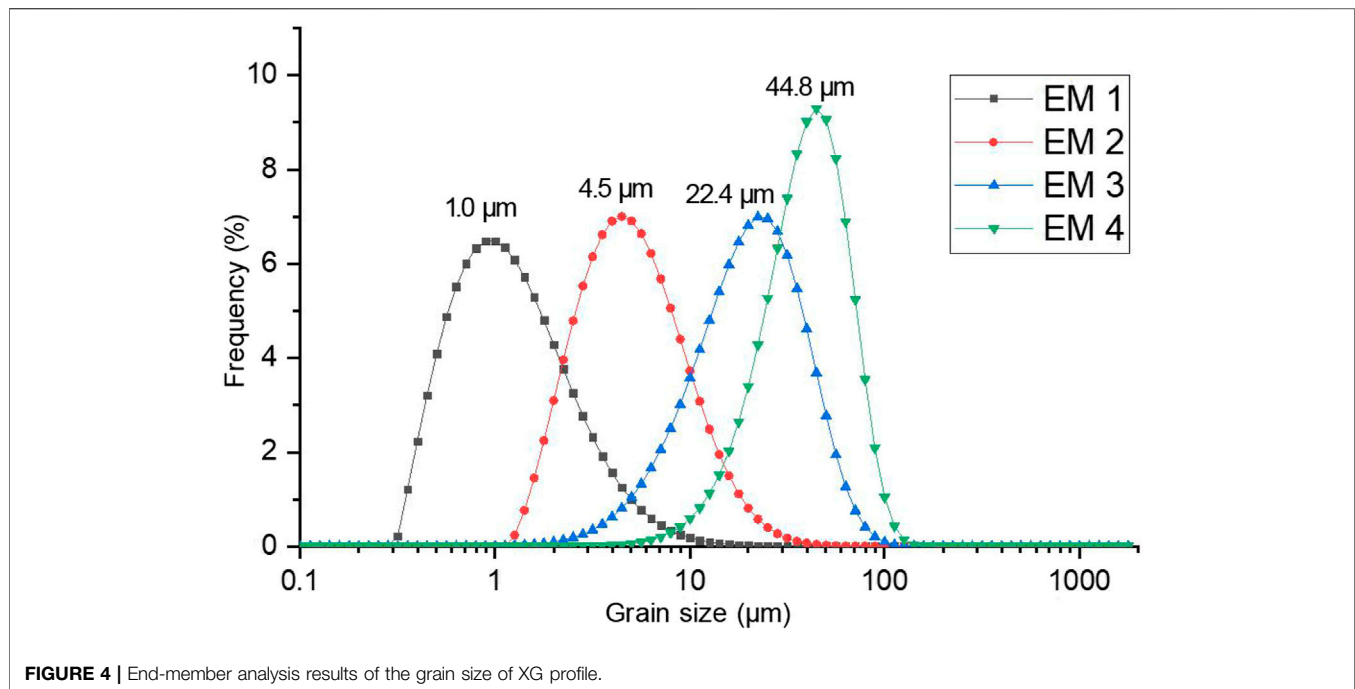
### Origin Identification by FLDA for XG Xiashu Loess

81 samples from XG profile were computed using the function, as shown in **Table 6**, all the samples from XG profile and ZKT profile are identified as ED, and all the floodplain deposit samples from NT profile are identified as FD. Therefore, the Xiashu loess in XG profile is considered as a eolian deposit.

### Genetic Interpretation of End-Members for XG Xiashu Loess

By end-member modeling analysis, the XG Xiashu loess profile was divided into four end-members (EM) (**Figures 4, 5**), from

EM1 to EM4, they account for 11.97, 23.06, 57.64, and 7.33% on average respectively (**Figure 5**). EM1 (modal size 1.0  $\mu\text{m}$ ) should be the product of weathering and pedogenesis after deposition. According to Tsoar and Pye (1987), dust particles  $>20\ \mu\text{m}$  are unlikely to be transported in long-term suspension across a large height range, and the  $>10\ \mu\text{m}$  components were regarded as nearby-source materials for Xiashu loess, whereas  $<5\ \mu\text{m}$  components were regarded as far-distant materials that was mainly derived from the arid regions of northwestern China by long-range transport (Wu et al., 2020). Therefore, we suggest that EM2 (modal size 4.5  $\mu\text{m}$ , accounting for 23.06%) represent the far-source materials that were mainly originated from the arid regions of NW China. EM3 (modal size 22.4  $\mu\text{m}$ , accounting for 57.64%) and EM4 (modal size 44.8  $\mu\text{m}$ , accounting for 7.33%) represent nearby-source materials that were mainly derived from local sources, which account for at least 64.97% in total and were presumed probably originated from the floodplains in the lower reaches of the Yangtze River, the Huai River, and the Yellow River to the north during glacial periods.



## Quartz Grain Surface Microtextural and Morphological Observations

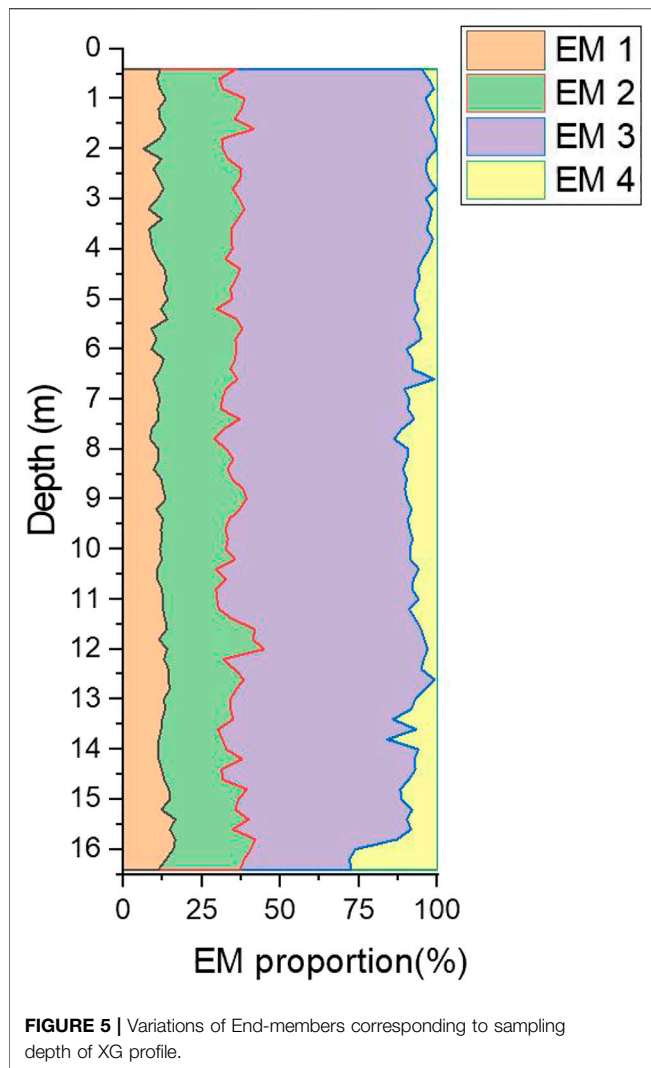
SEM observations of quartz grains from XG profile show that 55% grains observed are characterized by subangular outlines (Figures 6A,B, 7, 8), with a certain number of angular particles (29%) and round particles (5%) (Figure 8). The XG profile quartz grains show various shapes, such as plates, strips, triangles, cubes, pointed, slightly rounded, irregular, etc (Figures 6A,B). Mechanically produced features are abundant and varied, indicating that the quartz grains have experienced a range of external forces. Characteristics typical of eolian quartz grains in XG profile are common (Figures 6C–F), e.g. dish-shaped depressions (Figures 6C–F) and crescentic marks (Figure 6F) have occurrence rates 61% (Figure 8) and 48% (Figure 8), respectively. Other eolian features like upturned plates and meandering ridges (Figure 6D) also occurred on the grains, as well as pockmarks, formed pockmarked surfaces (Figures 6D,F), indicating quartz grain surface erosion during wind transportation. These features are similar to the microtextures characteristics in quartz grains from the loess on the CLP (Figure 9), reflecting transportation process by wind power. Meanwhile, many subaqueous features are also observed on the quartz grains: for example, V-shaped cracks (Figures 6G,I), grooves (Figure 6I), conchoidal fractures (Figure 6H), parallel striations caused by scratch (Figures 7C–E), triangular cracks (Figure 6H), underwater polished surfaces (Figures 7A,B,F), as well as bulbous edges and smooth edges (Figures 7E,G) caused by abrasion in subaqueous environments. V-shaped cracks, the most representative feature produced by grain-to-grain collisions in subaqueous environments (Mahaney, 2002; Krinsley and Doornkamp, 2011), reach an occurrence rate of 63%

in XG profile (Figure 8), suggesting a fluvial environment. A majority of quartz grains with high relief and abundant mechanical V-shaped cracks (Figures 6G–I), as well as parallel striations (Figures 7C–E) caused by scratch demonstrated that the quartz grains underwent a high-energy subaqueous transport. Some grains have surface microtextures that are typical of a subaqueous fluvial environment, with dish-shaped depressions or small impact pocks superimposed. This suggests the quartz grains were abraded in a fluvial environment before undergoing eolian transportation. In addition, 13% of the quartz grains (<20 μm) in XG profile have aeolian features and sharp edges on their surfaces, but without subaqueous characteristics, it is presumed that these grains were originated from far-distant materials. The grains in XG profile also exhibit silica dissolution and silica precipitation textures indicative of chemical weathering. Silica dissolution mainly comprise oriented etch pits (Figure 7H), solution pits and crevasses. Oriented etch pits are oriented and aligned, which are likely to be developed in rivers, lakes or marine environments, where the water affects the grains by dissolution (Mahaney, 2002; Krinsley and Doornkamp, 2011). 18% of the grains show oriented etch pits in XG profile, indicating a fluvial environment. Silica precipitation has produced silica globules (Figure 7I), silica pellicles and silica flowers, indicating that the quartz grains have undergone post-depositional weathering and pedogenesis.

## DISCUSSION

### Evidence of Aeolian Deposition

The XG profile and other reported Xiashu loess profiles present typical characteristics of eolian origin, including a uniform loose



and porous texture, massive structure, significant vertical joints, and disseminated iron-manganese films. The Xiashu loess covers hills, highlands, terraces, and other geomorphic units at varying elevations, and shows a range of origins and characteristics. In addition, the Xiashu loess strata are composed of alternating dark-colored (paleosol) and light-colored (loess) layers, resembling the typical loess-paleosol sequence on the CLP of northern China (Liu, 1985). Furthermore, although in some cases, the underlying strata of the Xiashu loess are composed of gravel layers, both of reported results and this study show that there are no sand layers or gravel layers in Xiashu loess profiles (Hao et al., 2010; Li et al., 2018b; Jiang et al., 2020). These depositional features distinguish aeolian deposits from fluvial deposits.

### Grain Size Evidence for the Provenance of XG Profile

The grain size composition of XG profile shows obvious aeolian characteristics, most notably the fine grain size and high clayey

silt fraction. Silt is the dominant component in all layers, with an average content of 68.82%, followed by clay and sand. The components with grain size  $< 50 \mu\text{m}$  in XG profile account for 93.16% on average. This clear dominance of the fine fraction ( $< 50 \mu\text{m}$ ) is considered to be a typical feature for eolian loess deposit (Liu, 1985; An et al. 1990; Guo et al. 2002). Coarse silt ( $50\text{--}10 \mu\text{m}$ ), which is the primary grain size group (average content 53.57%) (Table 5) in XG profile, is regarded as a key characteristic of aeolian loess on the CLP (Liu, 1985). The grain size compositions and grain size parameters of the loess are highly uniform between different layers of XG profile, suggesting that the Xiashu loess was likely to have been transported by a single external force. In addition, the grain size characteristics of loess in XG profile, Zhenjiang profile and Nanjing Zhoujiashan profile are strongly consistent, indicating a shared provenance (Li et al., 1997; Li et al., 2001b, Qiao et al., 2003, Hao et al., 2010; Jiang et al., 2020).

Due to the wind-sorting effect, prevailing northwesterly wind direction, and the decreasing carrying capacity with increasing distance from the source area, the grain size of loess on the CLP decreases from coarse to fine from northwest to southeast. Here, we choose two classical loess profiles on the CLP, one is Luochuan profile in the middle of the CLP, the other is Qinling profile in the southernmost part of the CLP. They are two representative profiles on the CLP. For example, the average grain size ( $M_z$ ) of the loess layers in Luochuan profile is  $6.01\phi$ , the mean value of that in other six loess profiles in the interior of the CLP is  $6.00\phi$  (Lei, 1998; Lei, 1999), indicating that the Luochuan profile is very representative. Here, we take Luochuan profile and Qinling profile in northern China as examples, the respective contents of sand ( $> 50 \mu\text{m}$ ) and clay ( $< 5 \mu\text{m}$ ) in Luochuan profile are 6.8 and 27.4% on average, the average grain size ( $M_z$ ) of Luochuan profile is  $6.01\phi$  (Liu, 1985; Lei, 1998; Lei, 1999). The respective values for the Qinling loess are 4.3%, 30.5%, and  $6.59\phi$  respectively, demonstrating the NW-SE trend toward finer grain sizes. The Xiashu loess is located far from northwest China; In addition, the warm-humid climate in the LRYR is highly conducive to post-depositional weathering and pedogenesis. Therefore, the sand content in the Xiashu loess should be lower than that of the loess on the CLP in northern China, while the contents of silt and clay materials should be higher. However, results show that sand ( $> 50 \mu\text{m}$ ) contents of the Xiashu loess in the LRYR, including XG (6.84%), Zhoujiashan of Nanjing (8.6%) and Zhenjiang (10.1%) are higher than those of the Luochuan profile (6.8%) and the Qinling profile (4.3%), while clay content in XG (24.3%), Zhoujiashan of Nanjing (21.3%) and Zhenjiang (19.1%) are lower than those in Luochuan (27.4%) and the Qinling loess (30.5%), so is the LGS Xiashu loess profile (24.9%) in East China Sea (Table 7). The average grain size of the loess layers in XG ( $6.42\phi$ , Paleosol layers not included) is coarser than that in Qinling loess ( $6.58\phi$ ) (Liu, 1985; Lei, 1998, Lei, 1999; Xu et al., 2016). All the characteristics above suggest that the grain size of the Xiashu loess in the LRYR does not follow the NW-SE trend of decreasing grain size. On the other hand, grains larger than  $20 \mu\text{m}$  are unlikely to be transported for long distances by wind. The components larger than  $20 \mu\text{m}$  in XG profile account for 38.92%, and sand content ( $> 50 \mu\text{m}$ ) accounts for 6.84%,

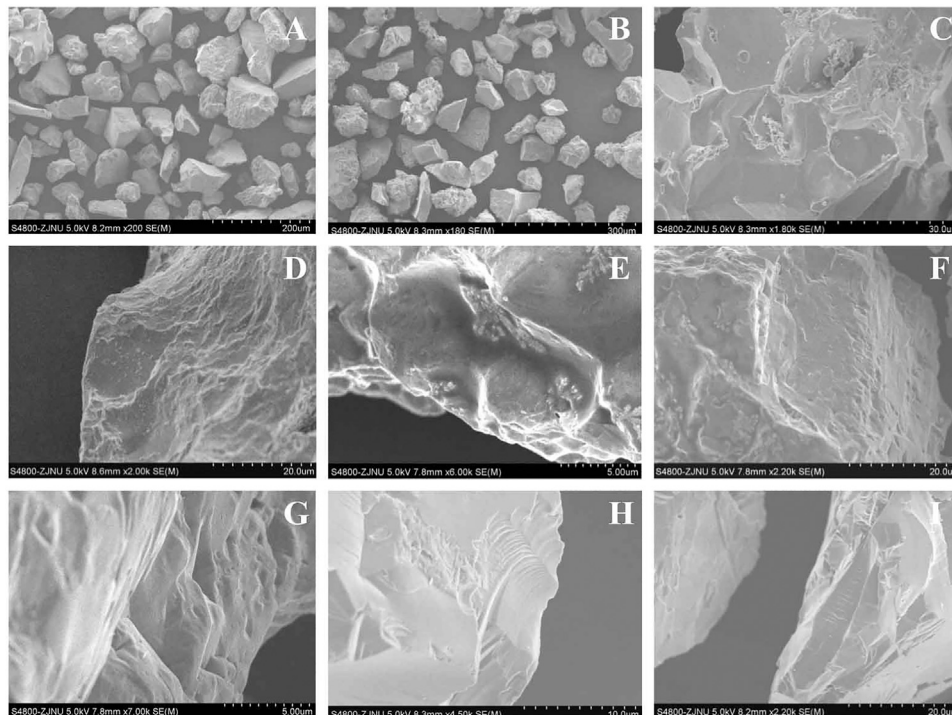


**FIGURE 6 | (A–B).** Quartz grains in XG profile. **(C).** Collision dish-shaped depressions are common on the surface. **(D).** Elongated dish-shaped depressions, meandering ridges, upturned plates and pockmarked surfaces. **(E)** Elongated dish-shaped depressions and crescentic marks. **(F).** Crescentic marks, dish-shaped depressions and pockmarked surfaces. **(G).** V-shaped cracks. **(H).** Conchoidal fractures, triangular cracks and underwater polished surfaces. **(I).** Grooves and V-shaped cracks.

especially the  $>10\ \mu\text{m}$  components, which were considered as nearby-source materials for the Xiashu loess (Wu et al., 2020), account for 60.51% in XG profile. In addition, end-member modeling analysis show that EM3 (modal size  $22.4\ \mu\text{m}$ , accounting for 57.64%) and EM4 (modal size  $44.8\ \mu\text{m}$ , accounting for 7.33%) represent nearby-source materials that were mainly derived from local sources, account for at least 64.97% in total. The relatively high content of grains  $>10\ \mu\text{m}$  and  $>20\ \mu\text{m}$  in XG profile is hard to explain using the distant source theory. In other words, nearby-source materials dominate the accumulation of the Xiashu loess. Finally, the poor sorting of XG and other reported Xiashu loess profiles in the LRYR is unusual (Li et al., 1997, Li et al., 2001b, Li et al., 2018b; Qiao et al., 2003; Xu et al., 2016), if the Xiashu loess was originated from the remote Gobi Desert of northwestern China or originated from the adjacent floodplains, it should have been well sorted. Therefore, multiple characteristics suggest that the Gobi Desert in inland NW China were not the primary source materials for the Xiashu loess, the Xiashu loess is probably a admixture composed of nearby-source materials and long-transport materials. Previous studies show that dust from inland NW China can be transported to the sea of Japan (Xiao et al., 1999), and the grain-size frequency curve of XG profile has also proved this point, so we suggest that a small amount of dust from the remote Gobi Desert in areas of northwestern China was likely to be transported to the LRYR

during glacial periods, and the poor sorting of XG profile and other reported Xiashu loess profiles is not difficult to understand.

### Quartz Grain Surface Microtextural Evidence for the Provenance of XG Profile

The loess on the CLP were originated from the remote Gobi Desert in inland northwestern China. The quartz grains in the loess are mostly subangular and angular, and with characteristic shapes (e.g. water drops, spears, diamonds, spindles or spirals) (Wang et al, 1985; Liu, 1985). These forms are mostly streamlined with a long primary axis, especially the twisted spiral shape representing the typical eolian loess on the CLP (Figure 9). This is because the quartz grains were carried by airflow for a long distance, and the grains themselves also rotated around their long axis, gradually being shaped by wind friction (Wang et al, 1985; Sun and An, 2000). Previous studies show that the quartz grains from the loess on the CLP are dominated by eolian features, subaqueous environmental characteristics are rare or absent (Liu, 1985; An et al., 1990; Ding et al., 1995; Guo et al., 2000). Our results show that most of the quartz grains of XG profile not only have typical features of wind transportation (such as dish-shaped depressions, crescentic marks and pockmarked surfaces), but also display a range of subaqueous environment characteristics (e.g. V-shaped cracks, subaqueous polished surfaces, grooves, etc) with high frequencies indicating that the grains have undergone

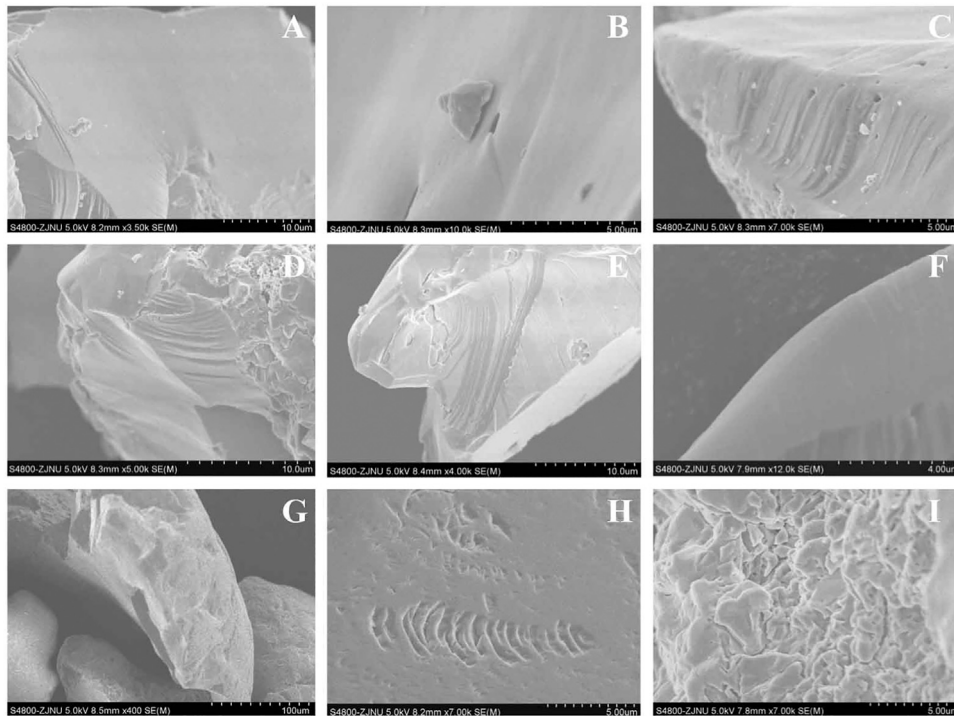


**FIGURE 7 | (A–B).** Underwater polished surfaces formed in subaqueous environment. **(C–E).** Parallel striations resulted from “grain-to-grain scratches” in subaqueous environment. **(F).** Polished surfaces and smooth edges caused by abrasion in subaqueous environment. **(G).** Smooth edges and V-shaped cracks. **(H).** Oriented etch pits. **(I).** Silica globules caused by precipitation.

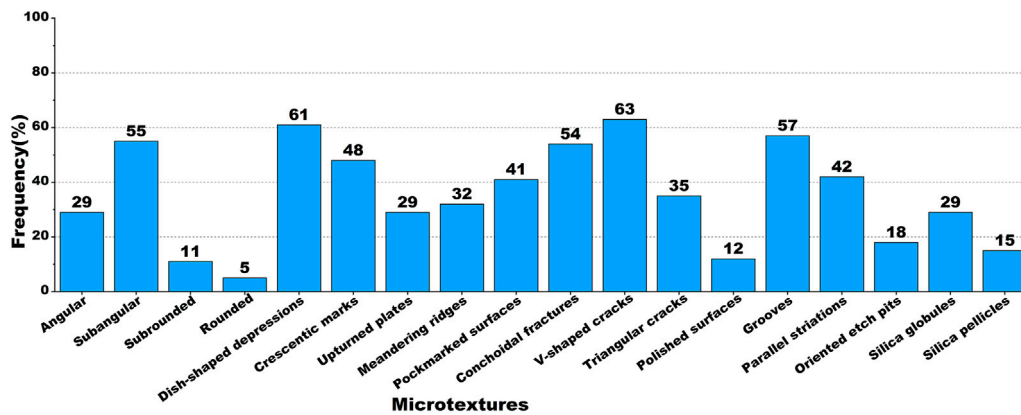
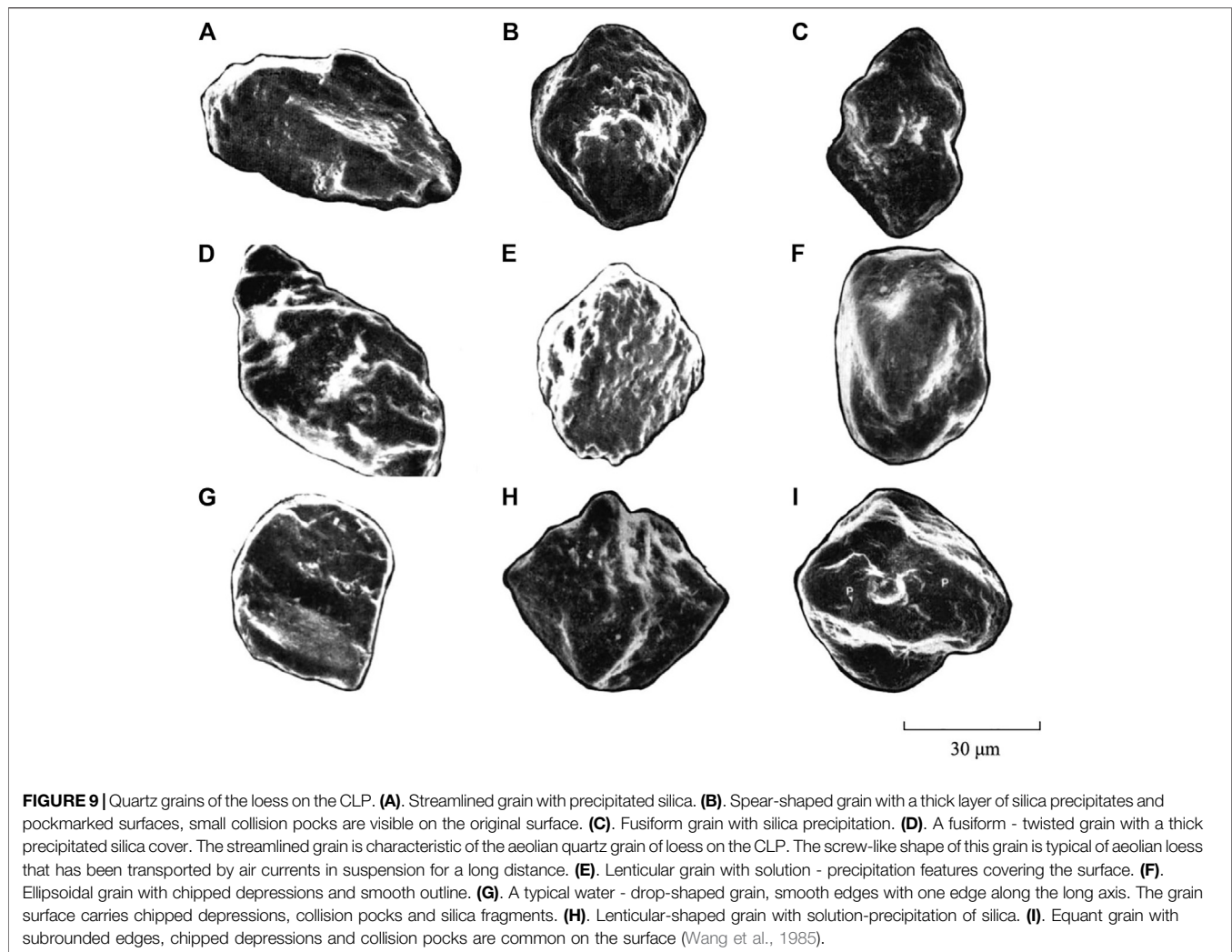


**FIGURE 8 |** Frequencies of different microtextures identified in XG profile.

subaqueous transport. Some grains with surface features of fluvial environments have aeolian characteristics superimposed on them, suggesting that the quartz grains were firstly abraded in a fluvial environment, and then transported and deposited by wind action. These features are distinctly different from those of the quartz grains on the CLP, and are also significantly different from those of the quartz grains derive from underlying parent rocks that are almost without any transportation and typically irregularly shaped with

sharp edges and extremely irregular shapes. In addition, if the Xiashu loess were originated from the remote Gobi Desert in inland of NW China, its quartz grains would have developed the same streamlined or spiral shapes as those of the loess on the CLP. However, SEM observations show that the quartz grains of XG profile present various shapes (such as plates, strips, triangles, cubes, points, and slightly rounded; and no screw-like grain occurs in the quartz grains observed), which were clearly distinct from the quartz grains on the



CLP. In addition, subaqueous environmental characteristics such as conchoidal fractures and V-shaped depressions are rare in typical eolian quartz grains, only can be seen in quartz grains that have just entered the eolian environment. The subaqueous environmental features in XG profile are abundant and clearly visible, indicating that the grains have been changed little by the eolian environment and have not been transported by wind for a long distance. Quartz grains  $>20\ \mu\text{m}$  are unlikely to be transported by wind over long distance and therefore are regarded as regional materials, SEM observations show that  $>20\ \mu\text{m}$  quartz grain (including sand grains) in XG profile are with obvious eolian features and subaqueous characteristics, indicating a near-source deposition. 13% of the quartz grains ( $<20\ \mu\text{m}$ ) observed have eolian features on their surfaces, but without subaqueous characteristics, it is presumed that these grains were originated from far-distant materials. These characteristics suggest that the Xiashu loess should be eolian deposit that was mainly originated from near-source materials. Previous studies show that dust from inland of NW China can be transported to the sea of Japan (Xiao et al., 1999), the grain-size frequency curve and the quartz grain microtextures, as

well as end-member modeling analysis indicate that the Xiashu loess may contain a certain amount of far-distant materials, so we suggest that nearby-source materials dominate the accumulation of the Xiashu loess, and the dust from the Gobi Desert in inland NW China have played a small role in the accumulation of the Xiashu loess. The surface microtextures and morphologies of the quartz grains provide a evidence for identifying the provenance of the Xiashu loess.

### Onset of Dust Accumulation in the LRYR and Its Environmental Significance

The accumulation of the Xiashu loess in the LRYR of southern China have significant environmental implications. In terms of sedimentary chronology, new advances in magnetostratigraphy and optically stimulated luminescence (OSL) dating have constrained the age of the lower boundary of the Xiashu loess to approximately 0.9 Ma, and the uppermost loess layer formed in the last glacial period (Qiao et al., 2003; Hao et al., 2010; Li et al., 2018b). The development of aeolian loess deposit in Asian

**TABLE 6** | The verification of the discriminant function.

Profile codes	No. of samples	Actual category	Discriminant results	
			ED	FD
ZKT	215	ED	215	0
NT	33	FD	0	33
XG	81	ED	81	0

subtropical regions since 0.9 Ma against a backdrop of global climate change. In the late Cenozoic, the overall climate trend was characterized by a global cooling, as evidenced by the expansion of continental ice sheets. This was accompanied by continental stepwise aridification, which led to the formation and development of the eolian loess deposit on the CLP (Liu, 1985; Guo et al. 1998; Sun and An, 2000; Guo 2010; Hao et al., 2010; Li et al., 2018b; Westerhold et al., 2020).

Great changes have taken place in global climate and environment in the middle of the Quaternary (Hao et al., 2010; Westerhold et al., 2020). The Mid-Pleistocene Transition (MPT) at about 1.25–0.7 Ma marked a shift in the primary climatic cyclicity from a 41 ka cycle to a 100 ka cycle, caused a significant increase in global ice volume and global cooling (Ruddiman et al., 1989; Clark et al., 2006; Hao et al., 2010; Elderfield et al., 2012; Westerhold et al., 2020). On the other hand, a significant tectonic movement (the “Kunlun–Yellow River movement”) on the Tibetan Plateau at about 1.2–0.6 Ma resulted in a period of rapid uplift. The “Kunlun–Yellow River Movement” raised the plateau and many surrounding mountains to a critical height of 3,500 m by around 0.9 Ma, causing widespread growth of glaciers which brought the Tibetan Plateau into the cryosphere and induced the first ice age in China since the Quaternary (Fang et al., 1996; Cui et al., 1998, Cui et al., 2011; Li et al., 2001a). The uplifted Tibetan Plateau serves as a cold source in winter and a heat source in summer, thereby intensifying both the winter monsoon and the summer monsoon, and also split the westerly jet into two streams. Thus resulted in the intensification and northward displacement of the Siberian high-pressure system. Global cooling and the uplifted Tibetan Plateau led to the enhancement of the Siberian high pressure, and caused a severe aridification in Asian interior and the intensification of the east Asian winter monsoon (Ruddiman

et al., 1989; Kutzbach et al., 1997). Hence, the dust deposition rate in northern China accelerated during 1.2–0.9 Ma, created extensive areas of eolian loess. The development of the exceptionally thick and coarse loess layers L15 (deposited at about 1.2 Ma) and L9 (deposited at about 0.9 Ma) on the CLP is a strong evidence for the cold-dry event in this period: L15 and L9 correspond to marine oxygen isotope stages 38 and 22, representing two periods of severe global cooling (Liu, 1985; Ding et al., 2002; Guo et al., 2000; Lu et al., 2000, Lu et al., 2008; Sun and Guo, 2017). Global cooling and the uplifted Tibetan Plateau also strongly influenced the LRYR region in southern China, resulting in a severe regional cooling and aridification. In addition, retreat of the coastline of the western Pacific Ocean increased the area of the continental land mass: for example, during the LGM, the coastlines of the East China Sea and the Yellow Sea had retreated eastwards by 6–7° of longitude (about 600 km), and the sea level had dropped by 150 m (Wang, 1999, Xu et al., 2012). The area of the LRYR, the Huai River and the Yellow River to the north is low, flat, and densely covered with rivers and lakes. In glacial periods, with declining of the sea level, the reduced river and lake levels yielded large areas of desiccated rivers, floodplains and lake beds, promoted these areas as a dust source for the accumulation of the Xiashu loess. The intensified winter monsoon produced strong wind erosion capacity and provided enough power to transport these regional fine materials, the river valleys and multistage river terraces of the Yangtze River and its tributaries provide good geomorphological conditions for loess deposition. The far-distant dust from the Gobi Desert of northwestern China may have played a small role in the accumulation of the Xiashu loess as well.

Sporopollen analysis of a typical loess stratum in Nanjing shows that herbaceous pollen dominated the total pollen assemblage, the sporopollen are mainly comprised of Compositae and Gramineae (subordinately artemisia and Chenopodiaceae), while arboreal pollen was mainly composed of Pinus, indicating a relatively arid and cold climate (Hao et al., 2010). The Ganzi loess in western Sichuan and the red earth in Chengdu plain (**Figure 1**) in the upper reaches of the Yangtze River have been confirmed as near-source eolian deposits formed in this period (Zhao et al., 2007; Qiao et al., 2007; Wang et al., 2018). The occurrence of sustained dust deposit reflects an important climate and environment change in the source and/or deposition regions (Pye, 1995). This means that the

**TABLE 7** | Comparison of grain size composition of loess in the LRYR and on the CLP (Li, 1998; Liu, 2006; Xu et al., 2016; Chen et al., 2017).

Sample sites	Clay (<5 μm)	Fine silt (5–10 μm)	Coarse silt (10–50 μm)	Sand (> 50 μm)
	%	%	%	%
XG, nanjing	24.3	15.3	53.6	6.8
ZJS, nanjing	21.3	15.6	54.5	8.6
CS, zhenjiang	19.1	14.8	56	10.1
DG, zhenjiang	28.4	18	49.4	4.2
LGS island	24.9	12.9	48.3	13.9
Qinling	30.5	16.9	48.3	4.3
Luochuan	27.4	12.5	53.3	6.8

environment of the whole Yangtze River Basin generally deteriorated at around 0.9 Ma. Therefore, we suggest that under the background of MPT, the strengthened east Asian winter monsoon and regional aridification driven by global cooling and the rapid uplift of the Tibetan Plateau are suggested as the primary drivers for the Xiashu loess. The development of the Xiashu loess was a regional response of the northern subtropical region in southern China to the MPT global cooling event.

## CONCLUSION

The grain size of the Xiashu loess in the LRYR do not follow the coarse-fine NW-SE trend of the loess deposit on the CLP, and the surface microtextures of the quartz grains in the Xiashu loess are mostly different from those on the CLP, indicating that the loess deposits in the two regions have different provenances. The Gobi Desert in inland NW China are not considered as the primary provenance for the Xiashu loess. Instead, the adjacent floodplains in the LRYR, the alluvial plains of the Huai River and the Yellow River to the north during glacial periods are suggested as the dominant source materials for the Xiashu loess. Regional aridification and a strengthened east Asian winter monsoon (driven by global cooling and the rapid uplift of the Tibetan

Plateau) are considered as the primary drivers for the accumulation of the Xiashu loess.

## DATA AVAILABILITY STATEMENT

The raw data supporting the conclusion of this article will be made available by the authors, without undue reservation.

## AUTHOR CONTRIBUTIONS

Investigation, QBF and LJ.; methodology, QBF and YL; data curation, QBF and XF.; writing original draft, QBF; review and editing, LJ and WY; funding acquisition, TW.

## FUNDING

This research was funded by the National Key and Program Of China (2016YFC0500909) "Key Techniques and Demonstration of Desertification Control in Semiarid Area in North China", and the National Key Research and Development Program of China (Grant No. 2017YFC0504804).

## REFERENCES

- An, Z. S., Liu, T. S., Lou, Y. C., Porter, S. C., Kukla, G., Xihao, W., et al. (1990). The long-term paleomonsoon variation recorded by the loess-paleosol sequence in Central China. *Quaternary international* 7-8, 91-95. doi:10.1016/1040-6182(90)90042-3
- Chen, Y., Li, X., Han, Z., Yang, S., Wang, Y., and Yang, D. (2008). Chemical weathering intensity and element migration features of the Xiashu loess profile in Zhenjiang, Jiangsu Province. *J. Geogr. Sci.* 18, 341-352. doi:10.1007/s11442-008-0341-9
- Chen, P. J., Zheng, X. M., and Zhou, L. M. (2017). Grain Size Distribution and Its Significance of the Xiashu Loess in Nanjing-Zhenjiang Area. *Geological Science and Technology Information* 34 (5), 8-13.
- Chen, R., Chen, J., Ma, J., and Cui, Z. (2019). Quartz Grain Surface Microtextures of Dam-Break Flood Deposits from a Landslide-dammed Lake: A case study. *Sedimentary Geology* 383, 238-247. doi:10.1016/j.sedgeo.2019.02.010
- Clark, P. U., Archer, D., Pollard, D., Blum, J. D., Rial, J. A., Brovkin, V., et al. (2006). The middle Pleistocene transition: Characteristics, mechanisms, and implications for long-term changes in atmospheric pCO<sub>2</sub>. *Quaternary Science Reviews* 25, 3150-3184. doi:10.1016/j.quascirev.2006.07.008
- Costa, P. J. M., Andrade, C., Dawson, A. G., Mahaney, W. C., Freitas, M. C., Paris, R., et al. (2012). Microtextural characteristics of quartz grains transported and deposited by tsunamis and storms. *sedimentary geology* 275-276, 55-69. doi:10.1016/j.sedgeo.2012.07.013
- Costa, P. J. M., Andrade, C., Mahaney, W. C., Marques da Silva, F., Freire, P., Freitas, M. C., et al. (2013). Aeolian microtextures in silica spheres induced in a wind tunnel experiment: Comparison with aeolian quartz. *Geomorphology* 180-181, 120-129. doi:10.1016/j.geomorph.2012.09.011
- Cui, Z., Wu, Y., Liu, G., Ge, D., Pang, Q., and Xu, Q. (1998). On Kunlun-Yellow River tectonic movement. *Sci. China Ser. D-Earth Sci.* 41, 592-600. doi:10.1007/bf02878741
- Cui, Z. J., Chen, Y. X., Zhang, W., et al. (2011). Glacial chronology and origins of Quaternary glaciations in China. *Quaternary sciences* 31, 749-764.
- Ding, Z., Liu, T., Rutter, N. W., Yu, Z., Guo, Z., and Zhu, R. (1995). Ice-Volume Forcing of East Asian Winter Monsoon Variations in the Past 800,000 Years. *Quat. res.* 44, 149-159. doi:10.1006/qres.1995.1059
- Ding, Z. L., Derbyshire, E., Yang, S. L., Yu, Z. W., Xiong, S. F., and Liu, T. S. (2002). Stacked 2.6-Ma grain size record from the Chinese loess based on five sections and correlation with the deep-sea  $\delta^{18}O$  record. *Paleoceanography* 17, 5-1. doi:10.1029/2001pa000725
- Ding, Z., Lu, R., and Wang, Y. (2019). Spatiotemporal variations in extreme precipitation and their potential driving factors in non-monsoon regions of China during 1961-2017. *Environmental Research Letters* 14, 024005. doi:10.1088/1748-9326/aaf2ec
- Ding, Z., Lu, R., Wang, L., Yu, L., Liu, X., Liu, Y., et al. (2021). Early-Mid Holocene climatic changes inferred from colors of eolian deposits in the Mu Us Desert. *Geoderma* 401, 115172. doi:10.1016/j.geoderma.2021.115172
- Elderfield, H., Ferretti, P., Greaves, M., Crowhurst, S., McCave, I. N., Hodell, D., et al. (2012). Evolution of ocean temperature and ice volume through the mid-pleistocene climate transition. *Science* 337, 704-709. doi:10.1126/science.1221294
- Fang, X. M., Chen, F. B., Shi, Y. F., and Li, J. J. (1996). Garze Loess and the Evolution of the Cryosphere on the Tibetan Plateau. *Journal of Glaciology and Geocryology* 18 (3), 193-200.
- Folk, R. L., and Ward, W. C. (1957). Brazos River bar [Texas]; a study in the significance of grain size parameters. *Journal of Sedimentary Research* 27 (1), 3-26. doi:10.1306/74d70646-2b21-11d7-8648000102c1865d
- Guo, Z. T. (2010). "22-8 Ma Monsoon evolution history recorded by eolian deposits (in Chinese)," in *Integrated Research on Environmental Evolution in Western China*. Editor Z. L. Ding (Beijing, China: China Meteorological Press), 1-19.
- Guo, Z., Liu, T., Fedoroff, N., Wei, L., Ding, Z., Wu, N., et al. (1998). Climate extremes in Loess of China coupled with the strength of deep-water formation in the North Atlantic. *Global and Planetary Change* 18, 113-128. doi:10.1016/s0921-8181(98)00010-1
- Guo, Z., Biscaye, P., Wei, L., Chen, X., Peng, S., and Liu, T. (2000). Summer monsoon variations over the last 1.2 Ma from the weathering of loess-soil sequences in China. *Geophys. Res. Lett.* 27, 1751-1754. doi:10.1029/1999gl008419
- Guo, Z. T., Ruddiman, W. F., Hao, Q. Z., Wu, H. B., Qiao, Y. S., Zhu, R. X., et al. (2002). Onset of Asian desertification by 22 Myr ago inferred from loess deposits in China. *Nature* 416, 159-163. doi:10.1038/416159a

- Hao, Q., Guo, Z., Qiao, Y., Xu, B., and Oldfield, F. (2010). Geochemical evidence for the provenance of middle Pleistocene loess deposits in southern China. *Quaternary Science Reviews* 29, 3317–3326. doi:10.1016/j.quascirev.2010.08.004
- Helland, P. E., Huang, P.-H., and Diffendal, R. F. (1997). SEM Analysis of Quartz Sand Grain Surface Textures Indicates Alluvial/Colluvial Origin of the Quaternary "Glacial" Boulder Clays at Huangshan (Yellow Mountain), East-Central China. *Quat. res.* 48, 177–186. doi:10.1006/qres.1997.1916
- Jiang, Q., Hao, Q., Peng, S., et al. (2020). Grain-size evidence for the transport pathway of the Xiashu loess in northern subtropical China and the linkage with fluvial systems. *Aeolian Research* 46, 1006–1013. doi:10.1016/j.aeolia.2020.100613
- Krinsley, D. H., and Doornkamp, J. C. (2011). *Atlas of quartz sand surface textures*. Cambridge, United Kingdom: Cambridge University Press.
- Kutzbach, J. E., Ruddiman, W. F., and Prell, W. L. (1997). "Possible effects of Cenozoic uplift and CO<sub>2</sub> lowering on global and regional hydrology," in *Tectonic Uplift and Climate Change*. Editor WF Ruddiman (New York, NY: Plenum Press), 149–170. doi:10.1007/978-1-4615-5935-1\_7
- Lai, Z. P., Zhou, J., and Xia, Y. F., (2001). Luminescence geochronology of Xiashu Loess near Nanjing. *Journal of Desert Research* 21, 116–121.
- Lei, X. Y. (1998). Research for the loss in Fengzhou, Qinling mountain. *Geology of Shanxi* 16 (2), 45–57.
- Lei, X. Y. (1999). Paleoenvironmental changes recorded by Shangzhou loess paleosol sequences on the eastern Qinling MTS. during the 0.6Ma. *Marine Geology & Quaternary Geology* 19 (1), 63–73.
- Li, L. W., Fang, Y. S., and Qiu, S. Z. (1978). Discovery and significance of the deer and cattle fossils in calcareous concretion of XiaShu formation in Laohushan, 1. Nanjing, China: J Nanjing Norm Univ-Nat Sci Ed, 22–26.
- Li, J. J., Fang, X. M., Pan, B., Zhao, Z., and Song, Y. (2001a). Late Cenozoic intensive uplift of Qinghai-Xizang Plateau and its imp-acts on environments in surrounding area. *Quaternary sciences* 21, 381–391.
- Liu, T. (1985). *Loess and the Environment*. Beijing, China: China Ocean Press.
- Li, C. Y., Peng, F., Xue, X., You, Q., Lai, C., Zhang, W., et al. (2018a). Productivity and Quality of Alpine Grassland Vary With Soil Water Availability Under Experimental Warming. *Frontiers in plant science* 9, 1790. doi:10.3389/fpls.2018.01790
- Li, C.-Y., Peng, F., Xue, X., Lai, C.-M., Zhang, W.-J., You, Q.-G., et al. (2021a). Degradation stage effects on vegetation and soil properties interactions in alpine steppe. *J. Mt. Sci.* 18, 646–657. doi:10.1007/s11629-020-6192-2
- Li, C., Peng, F., Lai, C., Xue, X., You, Q., Chen, X., et al. (2021b). Plant community changes determine the vegetation and soil δ<sup>13</sup>C and δ<sup>15</sup>N enrichment in degraded alpine grassland, *Land Degrad Dev* 32, 2371–2382. doi:10.1002/ldr.3912
- Li, X. S., Yang, D. Y., Lu, H. Y., and Han, H., (1997). The grain-size features of Quaternary aeolian-dust deposition sequence in south Anhui and their significance. *Marine Geology and Quaternary Geology* 17, 73–81.
- Li, X. S., Yang, D. Y., and Lu, H. Y. (2001b). Grain-size features and genesis of the Xiashu loess in Zhenjiang. *Marine Geology and Quaternary Geology* 21, 25–32.
- Li, X. S., Han, Z. Y., Lu, H. Y., Chen, Y., Yang, L., Xiaokong, Y., et al. (2018b). Onset of Xiashu loess deposition in southern China by 0.9 Ma and its implications for regional aridification. *Science in China* 48 (2), 210–223.
- Liu, F. (2006). *Paleo-Environmental Information study of Loess on Islands in East China Sea and Xiashu Loess[D]*. Shanghai, China: East China normal University.
- Lu, H., van Huissteden, K., Zhou, J., Vandenberghe, J., Liu, X., and An, Z. (2000). Variability of East Asian winter monsoon in Quaternary climatic extremes in North China. *Quat. res.* 54, 321–327. doi:10.1006/qres.2000.2173
- Lu, H. Y., Wang, X. Y., and Li, L. P. (2008). Aeolian dust records indicate the linkage of global cooling and Asian drying in late Cenozoic (in Chinese). *Quat Sci* 28, 949–956.
- Mahaney, W. (2002). *Atlas of Sand Grain Surface Textures and Applications*. Oxford, United Kingdom: Oxford University Press.
- Mahaney, W., and Kalm, V. (2000). Comparative scanning electron microscopy study of oriented till blocks, glacial grains and Devonian sands in Estonia and Latvia. *Boreas* 29, 35–51. doi:10.1111/j.1502-3885.2000.tb01199.x
- Mahaney, W. C., Stewart, A., and Kalm, V. (2001). Quantification of SEM microtextures useful in sedimentary environmental discrimination. *Boreas* 30, 165–171. doi:10.1080/030094801750203170
- Mahaney, W. C., Hancock, R. G. V., Milan, A., Pulleyblank, C., Costa, P. J. M., and Milner, M. W. (2014). Reconstruction of Wisconsin-age ice dynamics and compositions of southern Ontario glacial diamictons, glaciofluvial/lacustrine, and deltaic sediment. *Geomorphology* 206, 421–439. doi:10.1016/j.geomorph.2013.10.014
- Purtill, M. P., Kite, J. S., and Forman, S. L. (2019). Geochronology and Depositional History of the Sandy Springs Aeolian Landscape in the Unglaciated Upper Ohio River Valley, United States. *Front. Earth Sci.* 7, 322 doi:10.3389/feart.2019.00322
- Pye, K. (1987). *Aeolian Dust And Dust Deposits*. London, United Kingdom: Academic Press, 1–165.
- Pye, K. (1995). The nature, origin and accumulation of loess. *Quaternary Science Reviews* 14, 653–667. doi:10.1016/0277-3791(95)00047-x
- Qiao, Y., Guo, Z. T., Hao, Q. Z., Wu, W., Jiang, W., Yuan, B., et al. (2003). Loess-soil sequences in southern Anhui Province: magnetostratigraphy and paleoclimatic significance. *Chinese Sci Bull* 48, 2088–2093. doi:10.1360/03wd0183
- Qiao, Y. S., Zhao, Z. Z., and Li, Z. Y., (2007). Aeolian origin of The red earth formation in the Cheng Du Plain. *Quaternary Sciences* 27, 286–294.
- Ruddiman, W. F., Raymo, M., and McIntyre, A. (1989). Matuyama 41000-year: cycles: North Atlantic Ocean and northern hemisphere ice sheets. *Earth and Planetary Science Letters* 80, 117–129. doi:10.1016/0012-821X(86)90024-5
- Shi, Y., Zhang, W., and Dai, X., (2005). Characteristics of clay mineral assemblage of Xiashu Loess and their paleoenvironmental significance. *Marine Geology and Quaternary Geology* 25, 99–105.
- Smith, C., Soreghan, G. S., and Ohta, T. (2018). Scanning electron microscope (SEM) microtextural analysis as a paleoclimate tool for fluvial deposits: a modern test. *Geological Society of America Bulletin* 130, 1256–1272. doi:10.1130/b31692.1
- Sun, Y. B., and Guo, F. (2017). Rapid monsoon changes recorded by Chinese loess deposits. *Journal of Quaternary Science* 37 (5), 963–973. doi:10.11928/j.issn.1001-7410.2017.05.04
- Sun, Y. B., and An, Z. S. (2000). Sedimentary interpretation of surface textures of quartz grains from the eolian deposits. *Acta Sedimentologica Sinica* 18 (4), 506–510.
- Sweet, D. E., and Soreghan, G. S. (2010). Application of Quartz Sand Microtextural Analysis to Infer Cold-Climate Weathering for the Equatorial Fountain Formation (Pennsylvanian-Permian, Colorado, U.S.A). *Journal of Sedimentary Research* 80, 666–677. doi:10.2110/jsr.2010.061
- Westerhold, T., Marwan, N., Drury, A. J., Liebrand, D., Agnini, C., Anagnostou, E., et al. (2020). An astronomically dated record of Earth's climate and its predictability over the last 66 million years. *Science* 369, 1383–1387. doi:10.1126/science.aba6853
- Tsoar, H., and Pye, K. (1987). Dust transport and the question of desert loess formation. *Sedimentology* 34, 139–153. doi:10.1111/j.1365-3091.1987.tb00566.x
- Vandenberghe, J. (2013). Grain size of fine-grained windblown sediment: A powerful proxy for process identification. *Earth-Science Reviews* 121, 18–30. doi:10.1016/j.earscirev.2013.03.001
- Vandenberghe, J., Sun, Y., Wang, X., Abels, H. A., and Liu, X. (2018). Grain-size characterization of reworked fine-grained aeolian deposits. *Earth-Science Reviews* 177, 43–52. doi:10.1016/j.earscirev.2017.11.005
- Van Buuren, U., Prins, M. A., Wang, X. Y., Stange, M., Yang, X., and van Balen, R. T. (2020). Fluvial or aeolian? Unravelling the origin of the silty clayey sediment cover of terraces in the Hanzhong Basin (Qinling Mountains, central China). *Geomorphology* 367, 1–18. doi:10.1016/j.geomorph.2020.107294
- Vos, K., Vandenberghe, N., and Elsen, J. (2014). Surface textural analysis of quartz grains by scanning electron microscopy (SEM): from sample preparation to environmental interpretation. *Earth-Science Reviews* 128, 93–104. doi:10.1016/j.earscirev.2013.10.013
- Wang, Y., and Deonarine, B. (1985). *Model Atlas of Surface Textures of Quartz Sand[M]*. Beijing, China: Science Press.
- Wang, P. (1999). Response of Western Pacific marginal seas to glacial cycles: paleoceanographic and sedimentological features. *Marine Geology* 156, 5–39. doi:10.1016/s0025-3227(98)00172-8
- Wang, X., Lu, H., Zhang, H., Wu, J., Hou, X., Fu, Y., et al. (2018). Distribution, provenance, and onset of the Xiashu Loess in Southeast China with paleoclimatic implications. *Journal of Asian Earth Sciences* 155, 180–187. doi:10.1016/j.jseas.2017.11.022

- Wu, B Y. (1985). On depositional characteristic of Xiashu loess from Nanjing. *Marine Geology & Quaternary Geology* 5, 113–121.
- Wu, C., Zheng, X., Zhou, L., Ren, S., and Qian, P. (2020). Quantitative Estimation of Provenance Contributions to Loess Deposits in Eastern China and Implication for Paleo-dust Storm Activity. *Geomorphology* 373, 107489. doi:10.1016/j.geomorph.2020.107489
- Wu, C L, Zhu, C, and Lu, H Y, (2006). Magnetostratigraphic dating of the Xiashu loess in Nanjing area and its paleoenvironmental interpretation. *Journal of Stratigraphy* 30, 116–123.
- Xiao, J., and An, Z., (1999). Three large shifts in East Asian monsoon circulation indicated by loess -paleosol sequences in China and late Cenozoic deposits in Japan. *Palaeogeography, Palaeoclimatology, Palaeoecology*, 154(3), 179–189. doi:10.1016/s0031-0182(99)00110-8
- Xu, D., Lu, H., Wu, N., and Liu, Z., (2012). 30000-Year vegetation and climate change around the East China Sea shelf inferred from a high-resolution pollen record. *Quaternary International* 279-280, 543. doi:10.1016/j.quaint.2012.08.1908
- Xu, H. Y., Zheng, X. M., and Zhou, L. M., (2016). Characteristics of Quartz Grains of the Xiashu Loess in Zhoujiashan Nanjing and Its Provenance Significance. *Acta Sedimentologica Sinica* 34 (6), 1176–1186.
- Yang, L. H., Ye, W., and Zheng, X. M., (2014). The Discriminant Function with Grain Size of Floodplain and Aeolian Sediments and Its Application in the Quaternary Red Clay. *Geographical Research* 33 (10), 1848–1856. doi:10.11821/dlyj201410006
- Yang, L.-H., Zheng, X.-M., Ye, W., et al. (2017). Sedimentary environment of vermicular red clay in South China. *J. Mt. Sci.* 14 (3), 513–526. doi:10.1007/s11629-016-3973-8
- Yang, S. Y., Li, C. X., Yang, D. Y., and Li, X. S. (2004). Chemical weathering of the loess deposits in the lower Changjiang Valley, China, and paleoclimatic implications. *Quaternary International* 117, 27–34. doi:10.1016/s1040-6182(03)00113-7
- Yang, X., Wang, X., Van Balen, R. T., Prins, M. A., Wang, S., van Buuren, U., et al. (2019). Fluvial terrace formation and its impacts on early human settlement in the Hanzhong basin, Qinling Mountains, central China. *Global and Planetary Change* 178, 1–14. doi:10.1016/j.gloplacha.2019.04.007
- Zhang, W., Yu, L., Lu, M., Zheng, X., and Shi, Y. (2007). Magnetic properties and geochemistry of the Xiashu Loess in the present subtropical area of China, and their implications for pedogenic intensity. *Earth and Planetary Science Letters* 260, 86–97. doi:10.1016/j.epsl.2007.05.018
- Zhang, W., Yu, L., Lu, M., Zheng, X., Ji, J., Zhou, L., et al. (2009). East Asian summer monsoon intensity inferred from iron oxide mineralogy in the Xiashu Loess in southern China. *Quaternary Science Reviews* 28, 345–353. doi:10.1016/j.quascirev.2008.10.002
- Zhao, Z Z, Qiao, Y S, Wang, Y, Fu, J., Wang, S., Li, C., et al. (2007). Magnetostratigraphy and its Paleoclimatic Significance Of The Red Earth Formation In The Cheng Du Plain. *Science in China, Series D* 37, 370–377.
- Zheng, X M. (1999). *Aeolian Deposition and Environment in Changjiang Delta and Extending Sea Areas*. Shanghai, China: East China Normal University Press.

**Conflict of Interest:** The authors declare that the research was conducted in the absence of any commercial or financial relationships that could be construed as a potential conflict of interest.

Copyright © 2021 Fan, Liao, Li, Ye, Wang and Feng. This is an open-access article distributed under the terms of the Creative Commons Attribution License (CC BY). The use, distribution or reproduction in other forums is permitted, provided the original author(s) and the copyright owner(s) are credited and that the original publication in this journal is cited, in accordance with accepted academic practice. No use, distribution or reproduction is permitted which does not comply with these terms.